Electronic Supplementary Information (ESI)

for

Evolution of Mn-Bi_2O_3 from the Mn-doped Bi_3O_4Br electro(pre)catalyst during the oxygen evolution reaction

Avinava Kundu[#†], Ashish Kumar Dhillon[#†], Ruchi Singh[†], Sanmitra Barman*[‡], Soumik Siddhanta*[†] and Biswarup Chakraborty*[†]

[†]Department of Chemistry, Indian Institute of Technology Delhi, Hauz Khas, 110016, New Delhi, India

[‡]Center for Advanced Materials and Devices (CAMD), BML Munjal University, Haryana, India

[#] Authors contributed equally

Department of Chemistry, Indian Institute of Technology Delhi, Hauz Khas, 110016, New Delhi, India

*sanmitra.barman@bmu.edu.in, *soumik@chemistry.iitd.ac.in and *cbiswarup@chemistry.iitd.ac.in

Table of Contents

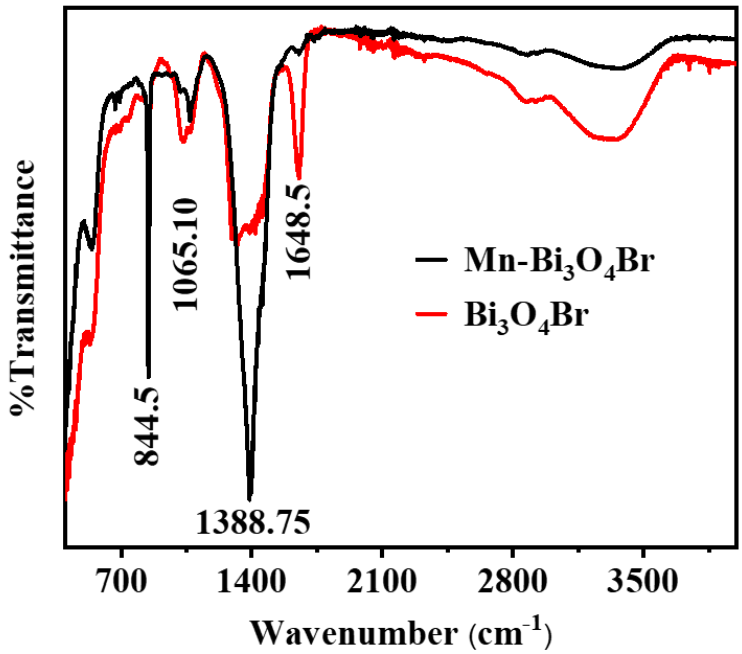

Figure S1: FTIR spectra recorded for Mn-Bi_3O_4Br and Bi_3O_4Br powder sample.

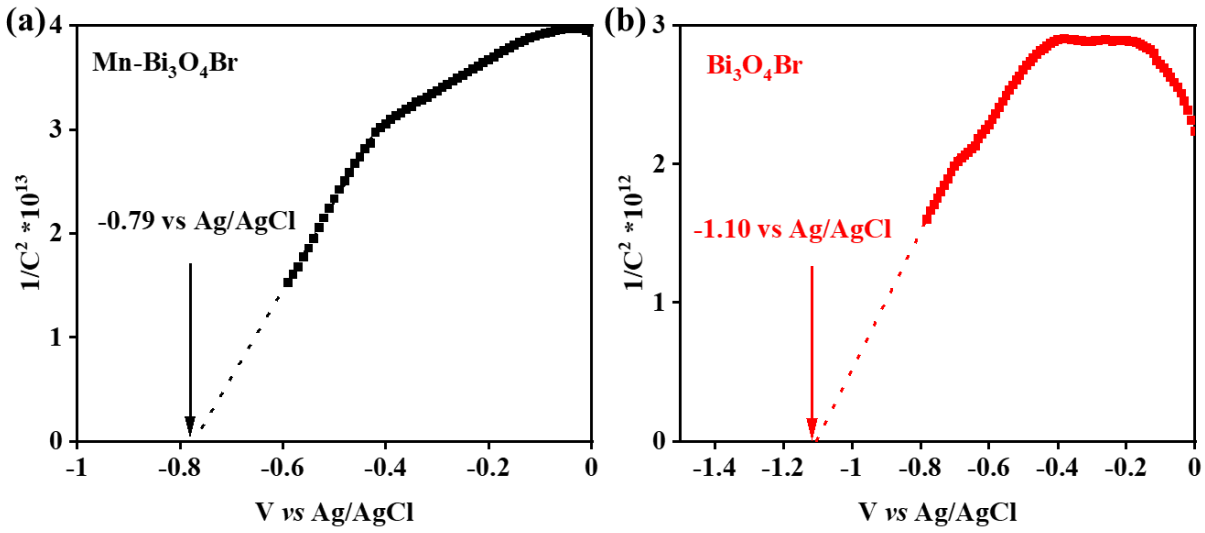

Figure S2: Mott-Schottky analysis of the (a) Mn-Bi_3O_4Br and (b) Bi_3O_4Br powder samples.

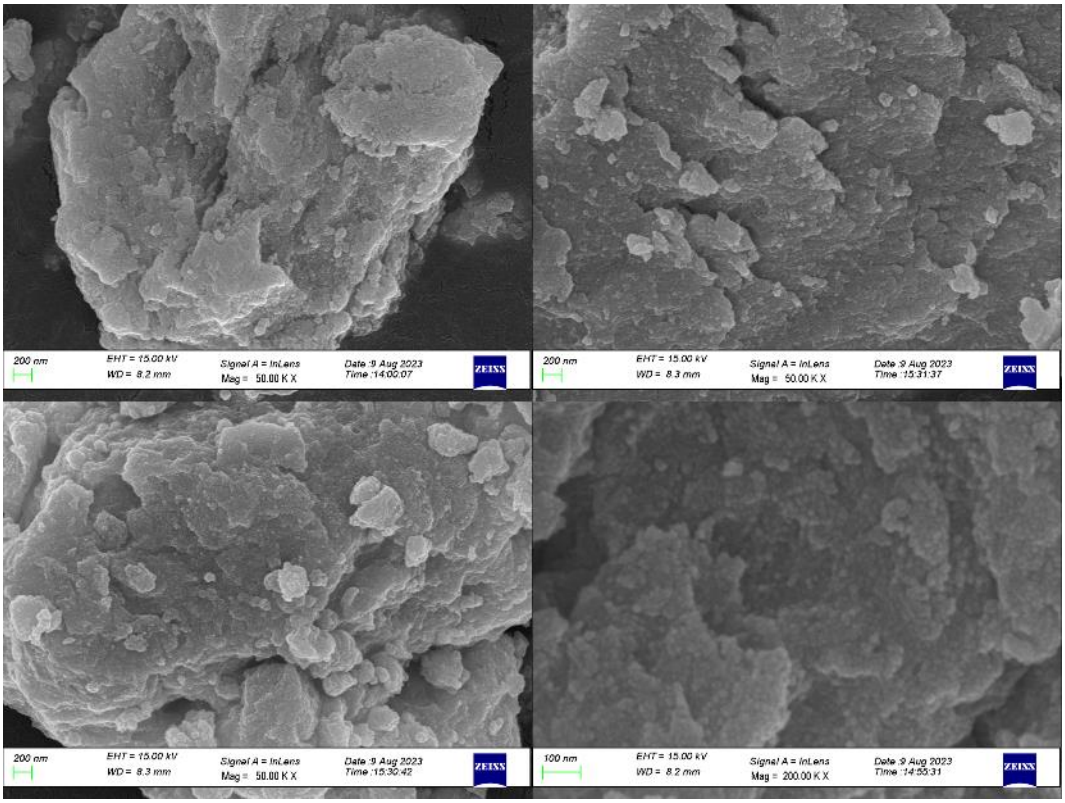

Figure S3: FESEM images of the Mn-Bi_3O_4Br collected at different magnification confirming the layered type structure.

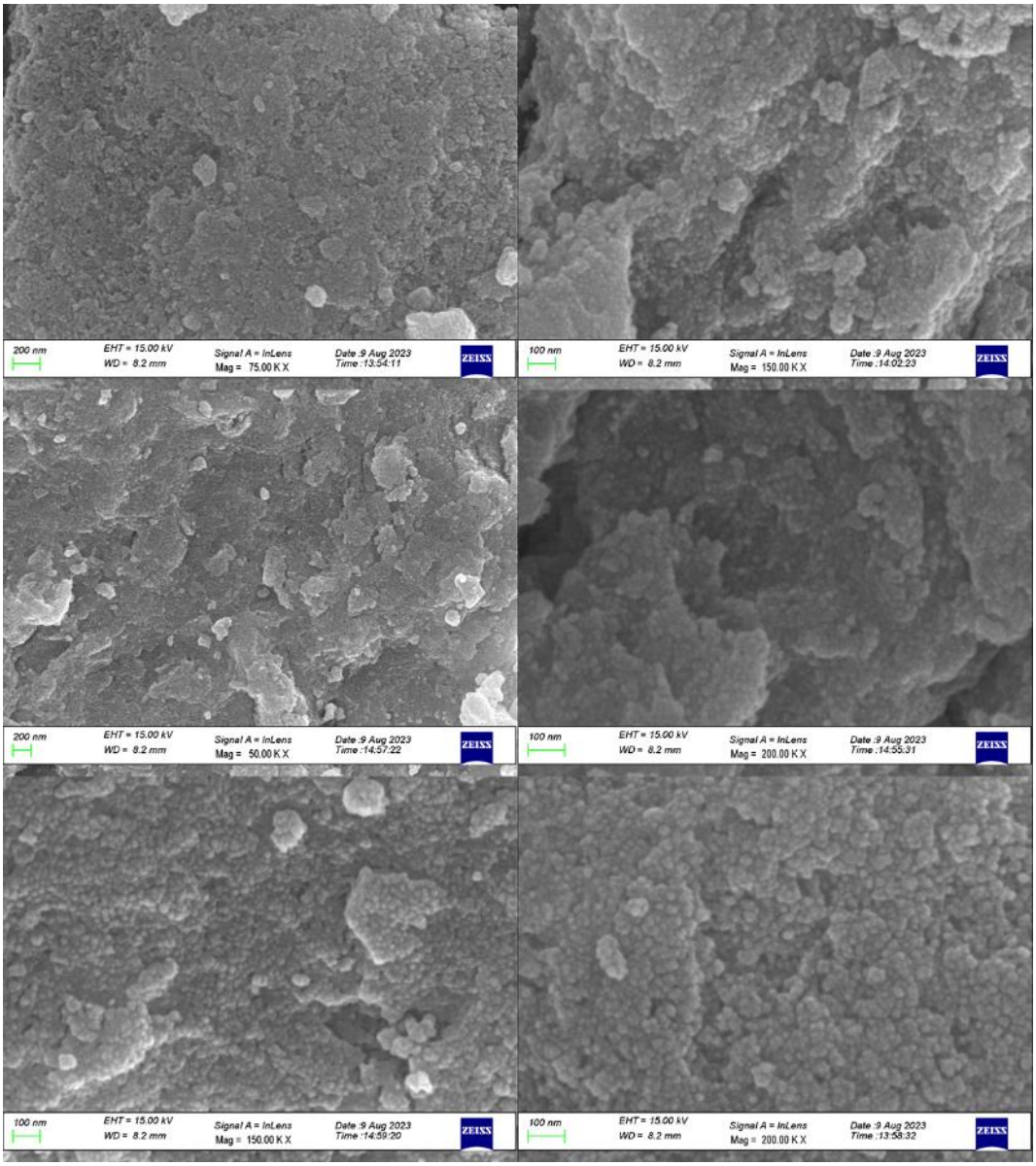

Figure S4: FESEM images of pristine Bi_3O_4Br powder samples in different magnifications and different places of bulk materials.

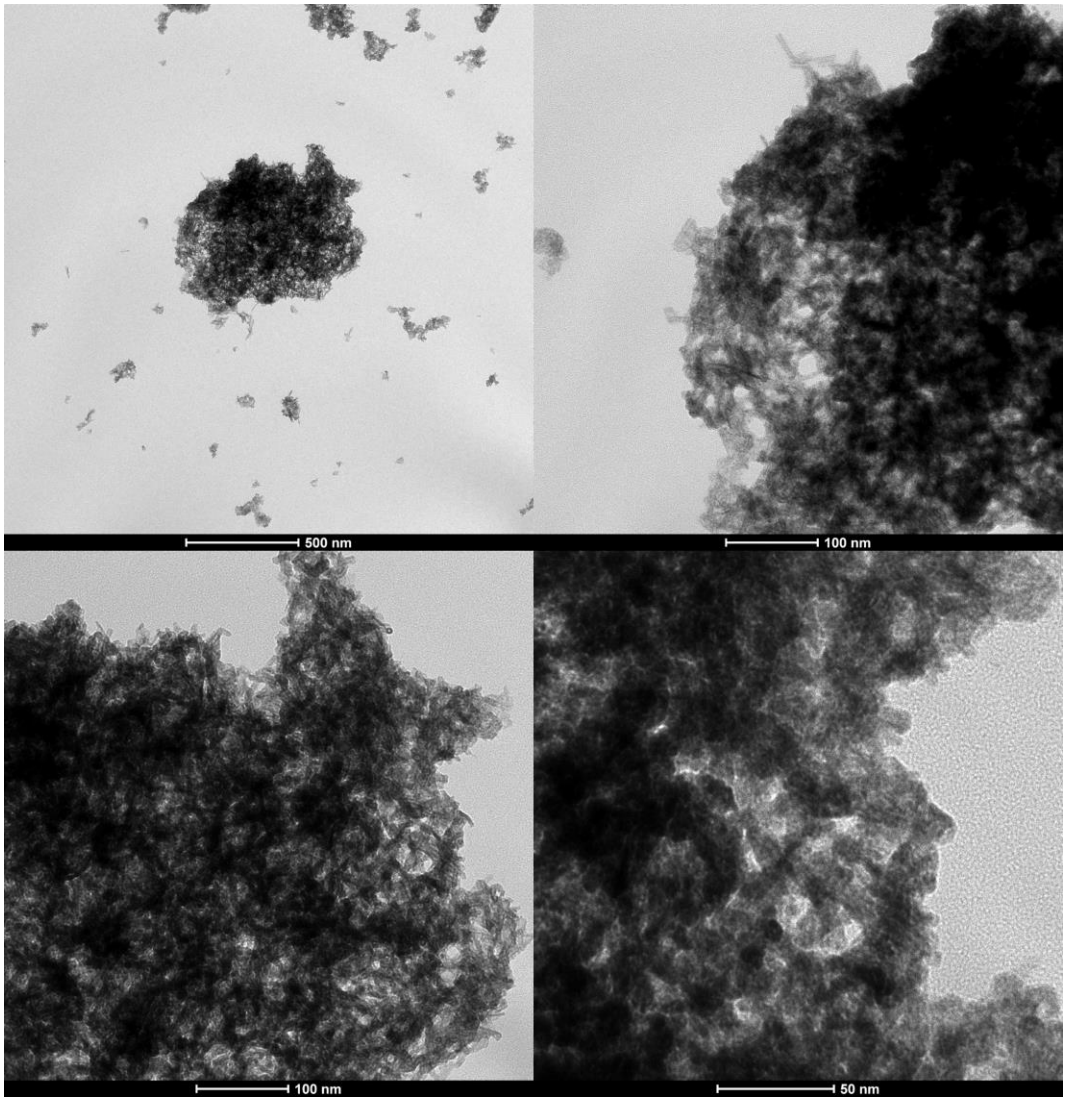

Figure S5: TEM images of pristine Bi_3O_4Br powder samples with different magnifications.

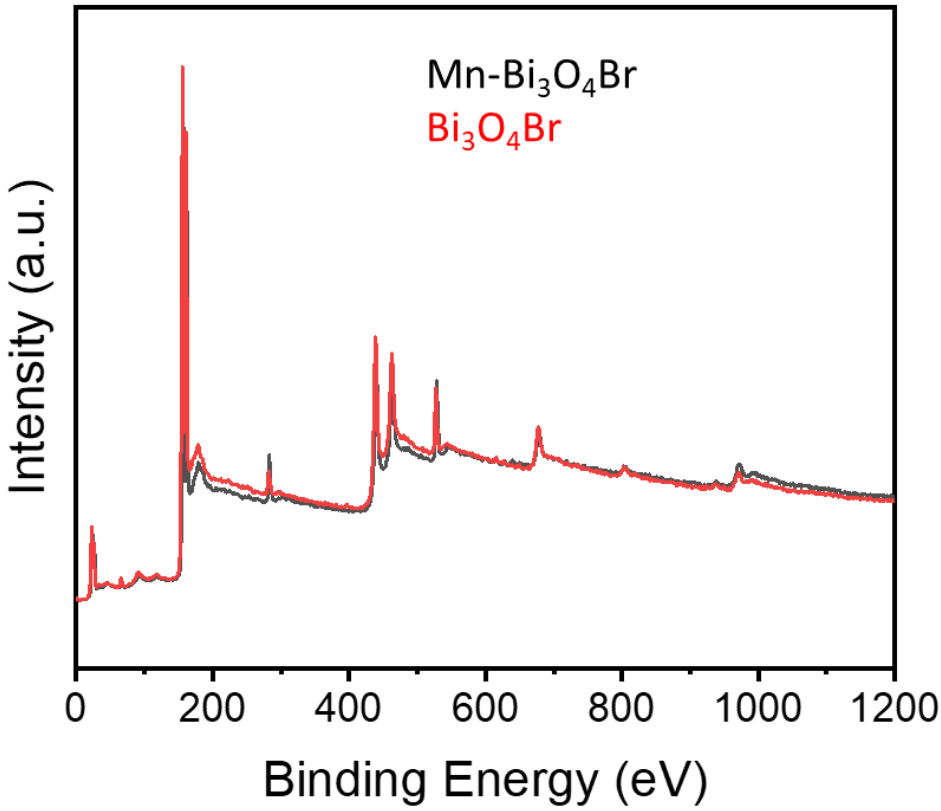

Figure S6: XPS survey spectra recorded for Mn-doped Bi_3O_4Br and pristine Bi_3O_4Br powder sample.

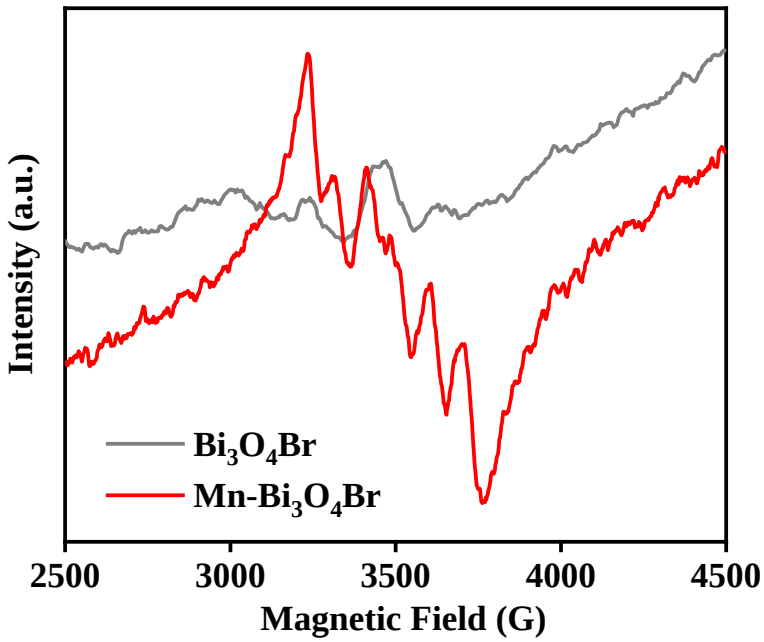

Figure S7: X-band (9.4 GHz) EPR spectra of Mn-Bi_3O_4Br (red) and Bi_3O_4Br (grey), recorded at room temperature.

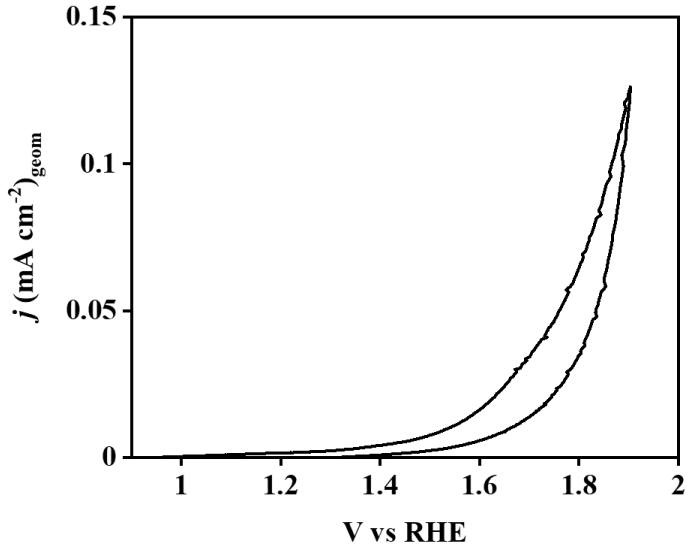

Figure S8: CV scan recored with Bi_3O_4Br on GC electrode within a potential window of 0.9 to 1.9 V vs RHE. (Scan starts and ends: 0.9 V, potential switch: 1.9 V, scan rate 5 mV s^{-1}, 1 M KOH as electrolyte, without iR-correction)

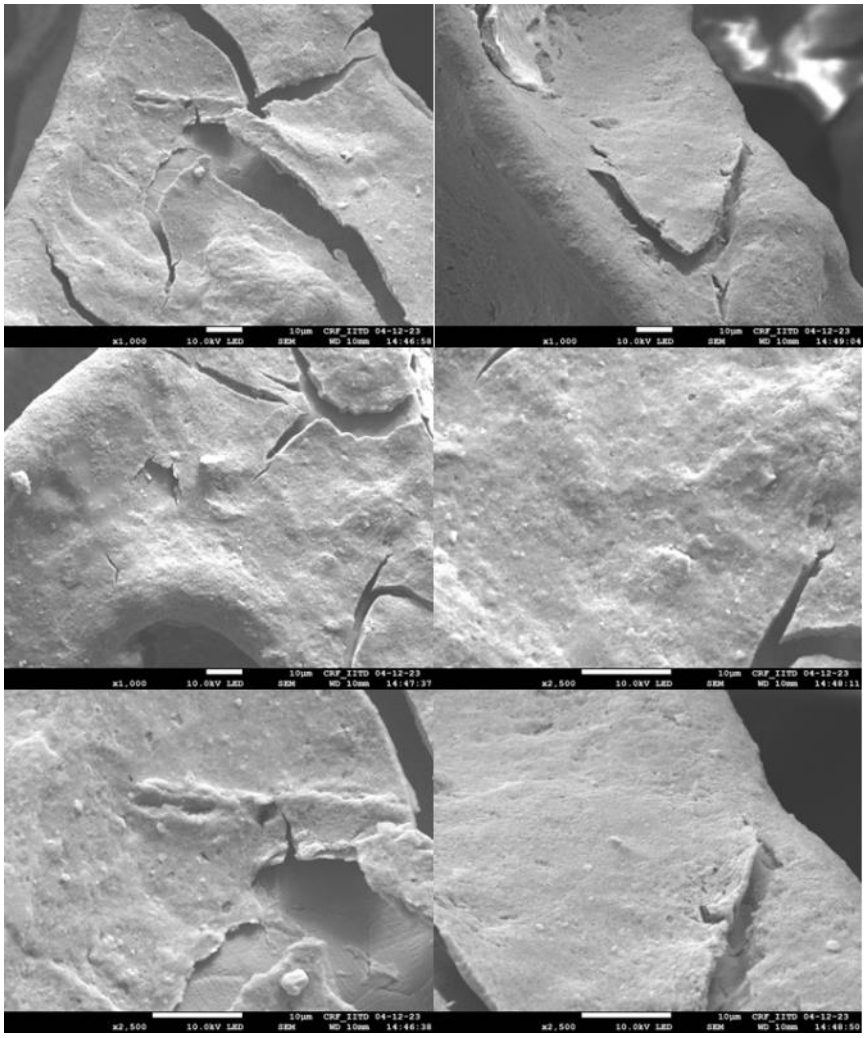

Figure S9: FESEM images (at different magnifications) of the Mn-Bi_3O_4Br sample drop-casted on the nickel foam.

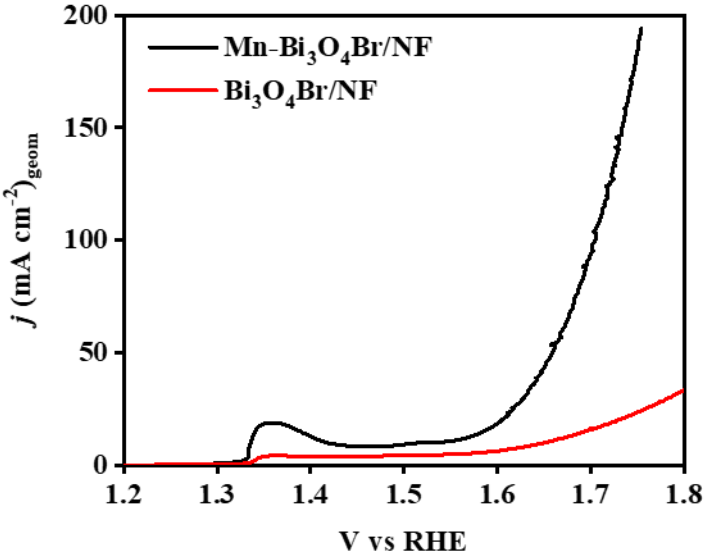

Figure S10: LSV study recorded in between 1.2 to 1.8 V vs RHE for Mn-Bi_3O_4Br and Bi_3O_4Br/NF using graphite rod as a counter electrode.

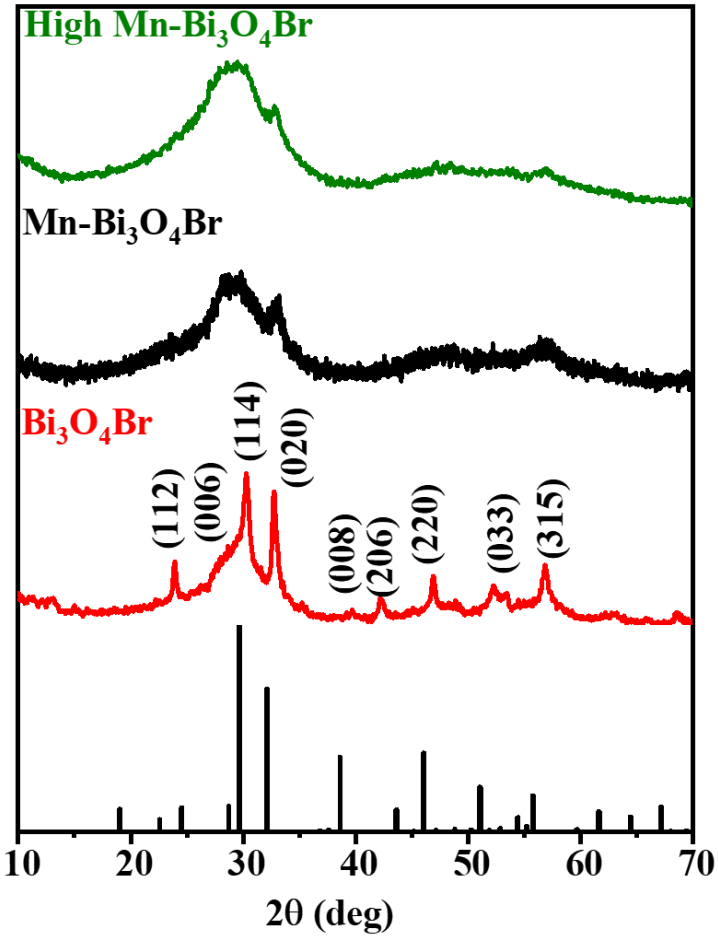

Figure S11: Powder X-ray diffraction pattern of the as-synthesised Bi_3O_4Br (red), Mn-Bi_3O_4Br (black) and a different Mn-containg Bi_3O_4Br labelled as high Mn- Bi_3O_4Br (green). Black bars at the bottom ICDD data (84-0793) of Bi_3O_4Br.

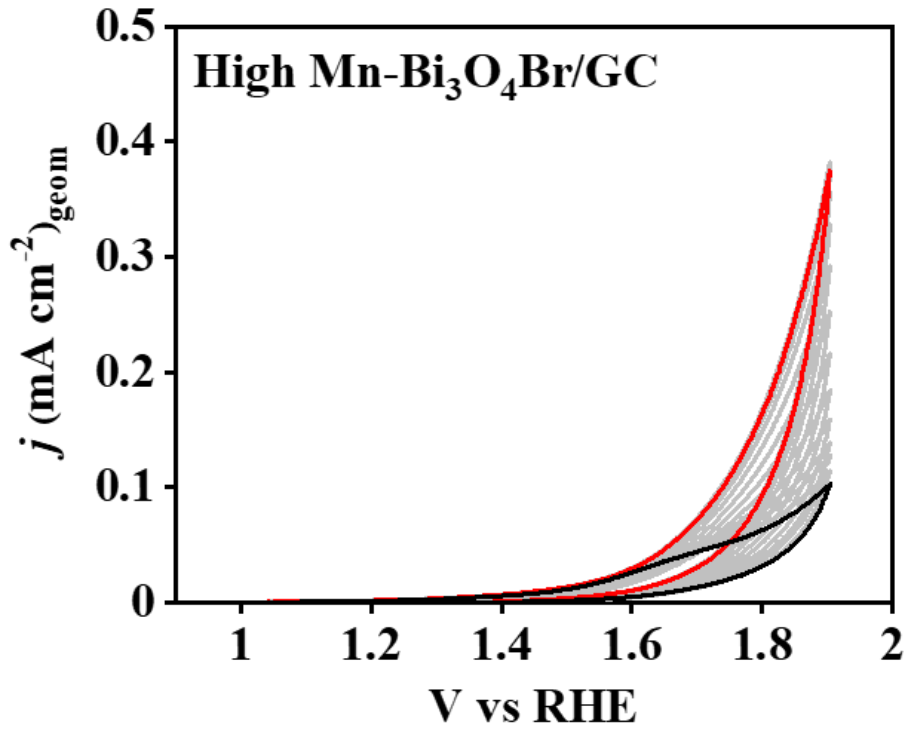

Figure S12: CV cycles of the different amount of Mn-doped in Bi_3O_4Br sample (labelled as high Mn-Bi_3O_4Br) on GC electrode. (Scan starts and ends: 0.9 V, potential switch: 1.9 V, scan rate 5 mV s^{-1}, 1 M KOH as electrolyte)

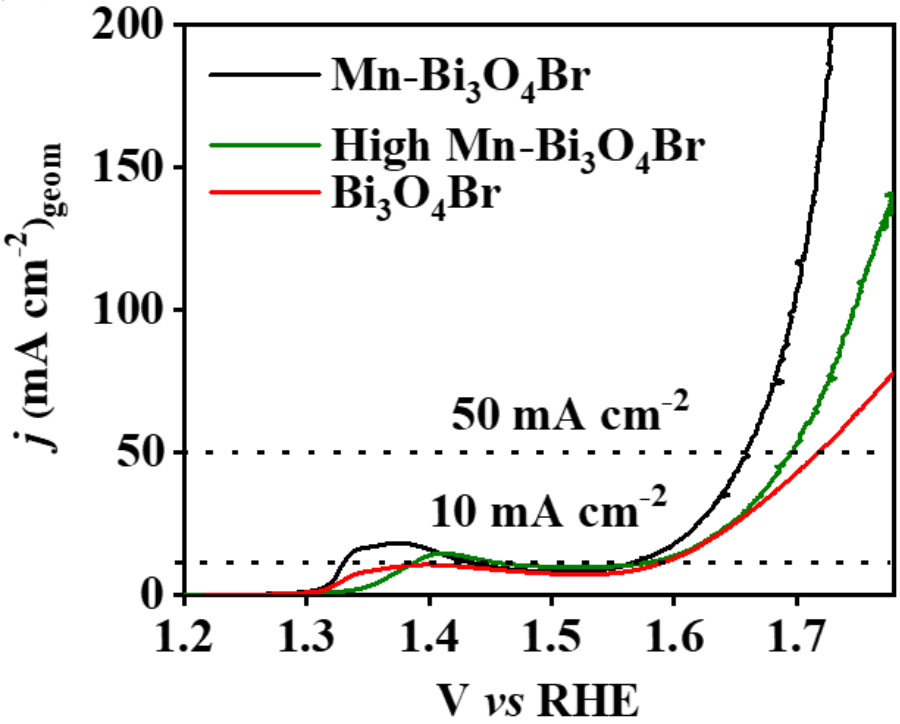

Figure S13: Comparison of polarograms obtained from the linear sweep voltammetry (LSV) recorded in between 1.2 to 1.8 V vs RHE for Mn-Bi_3O_4Br/NF, High Mn-Bi_3O_4Br/NF and Bi_3O_4Br/NF.

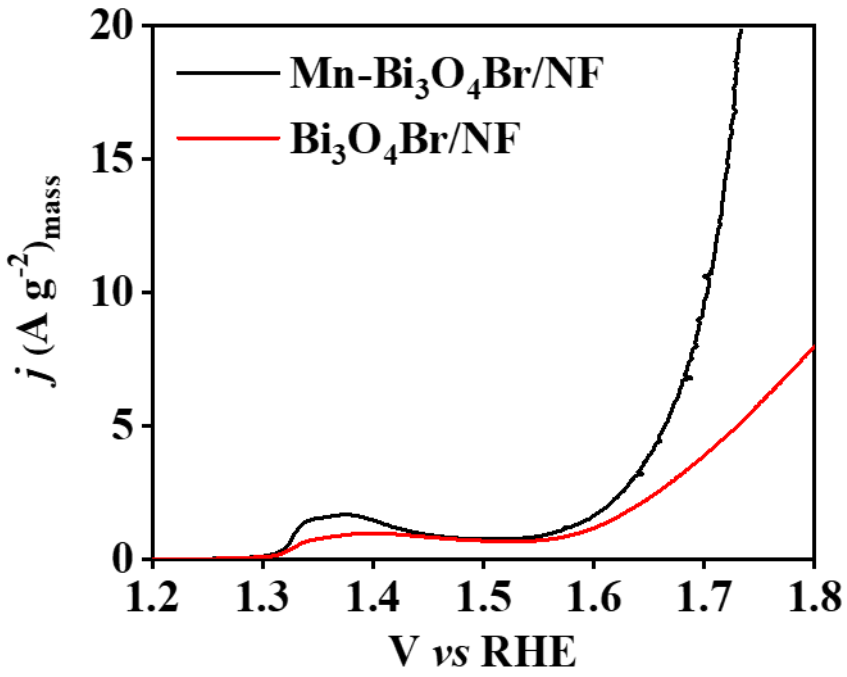

Figure S14: Mass activity of the Mn-Bi_3O_4Br/NF and Bi_3O_4Br/NF electrode.

Table S1. Performance of 7% Mn doped Bi_3O_4Br and comparision of different pure Mn-based OER electrocatalysts.

Catalyst	Electrolyte	Overpotential	Reference
Mn-Bi_3O_4Br	1 M KOH	337	This Work
Metal-doped MnO_2	1 M KOH	390	[1]
α-MnO_2	0.1 M KOH	508	[2]
MnO_x NWs	0.1 M KOH	519	[3]
Ni–MnO_2	1 M KOH	330	[4]
α-MnS	1 M KOH	292	[5]
MnO_2/CQD	1 M KOH	343	[6]
MnSe/CC	1 M KOH	310	[7]
MnSe@MWCNT/CC	1 M KOH	290	[7]
MnO_x/OCNT	0.1 M KOH	520	[8]
$MnGa_4$	1 M KOH	291	[9]
$LiMn(H_2O)_2[BP_2O_8]$	1 M KOH	228	[10]

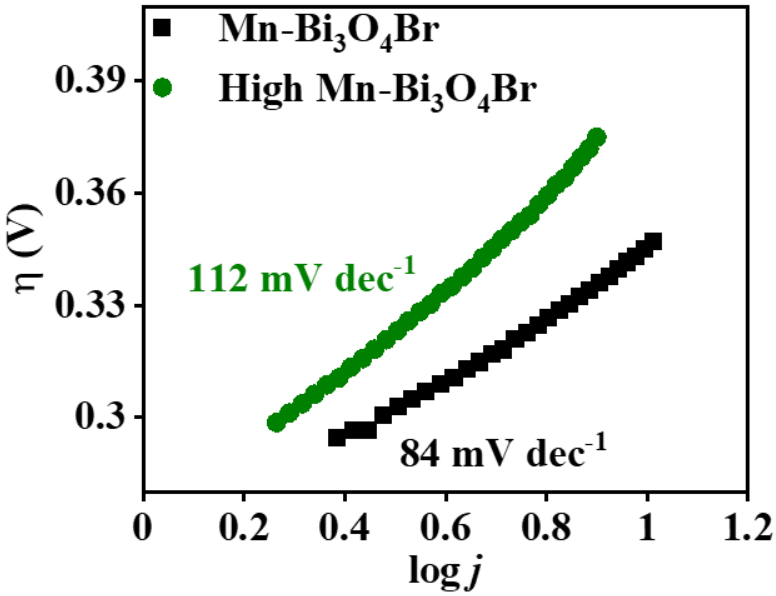

Figure S15: Tafel slope analysis of the Mn-Bi_3O_4Br/NF and High Mn-Bi_3O_4Br/NF electrode obtained from the LSV curves.

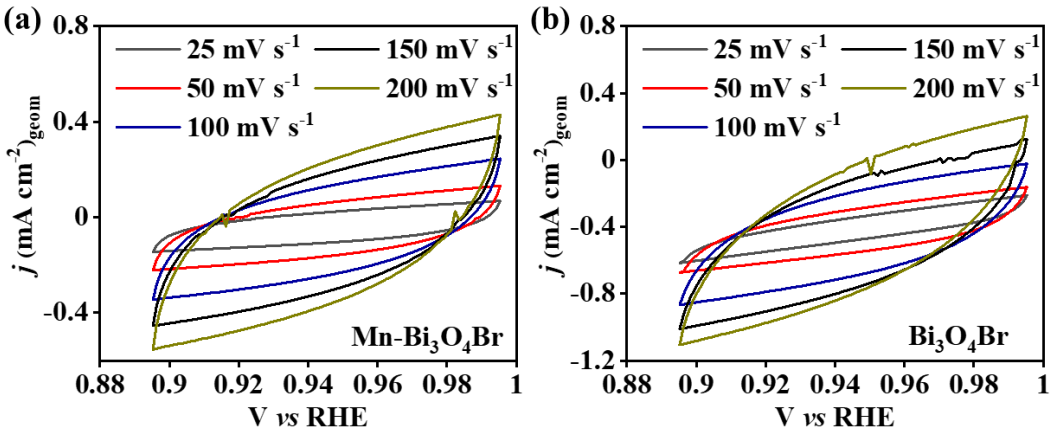

Figure S16: CV cycles recorded in between 0.89 V and 0.99 V vs RHE (in the capacitive region) for (a) Mn-Bi_3O_4Br/NF and (b) Bi_3O_4Br/NF. The scan rate was varied from 25 mV s^{-1} to 200 mV s^{-1}.

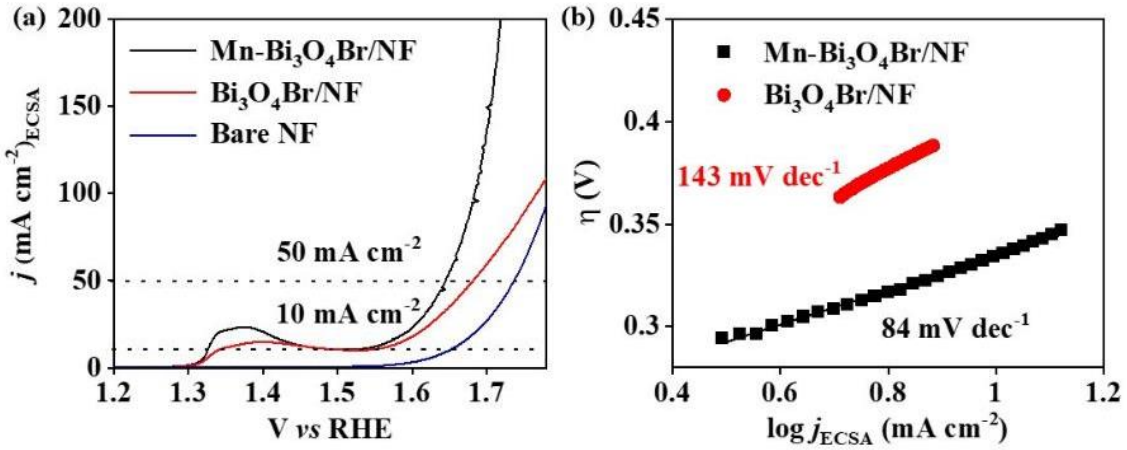

Figure S17: (a) ECSA normalized polarization curves, and (b) corresponding Tafel plot for Mn-Bi_3O_4Br, Bi_3O_4Br, and bare NF.

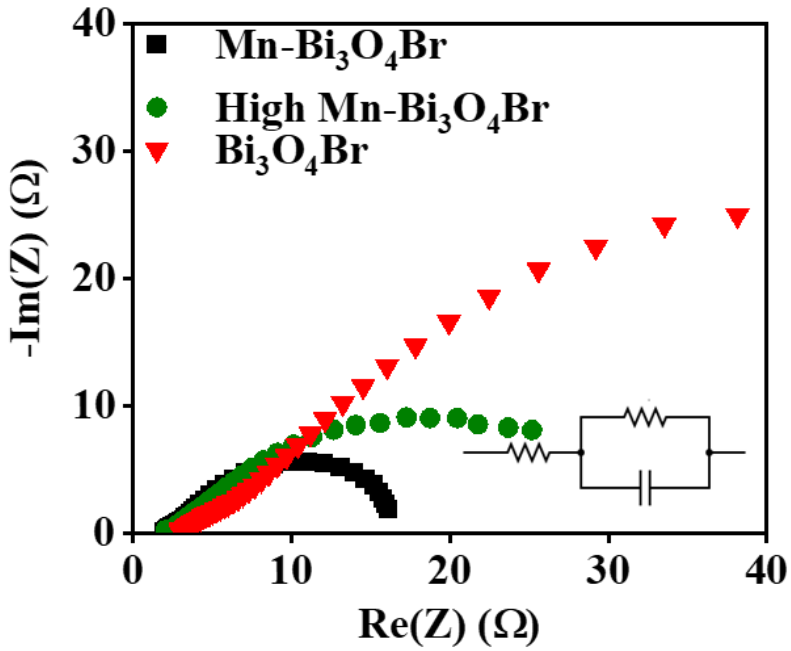

Figure S18: Nyquist plot from the data obtained from the EIS recorded in between 100 kHz and 0.01 Hz frequency range with Mn-Bi_3O_4Br, High Mn-Bi_3O_4Br and Bi_3O_4Br.

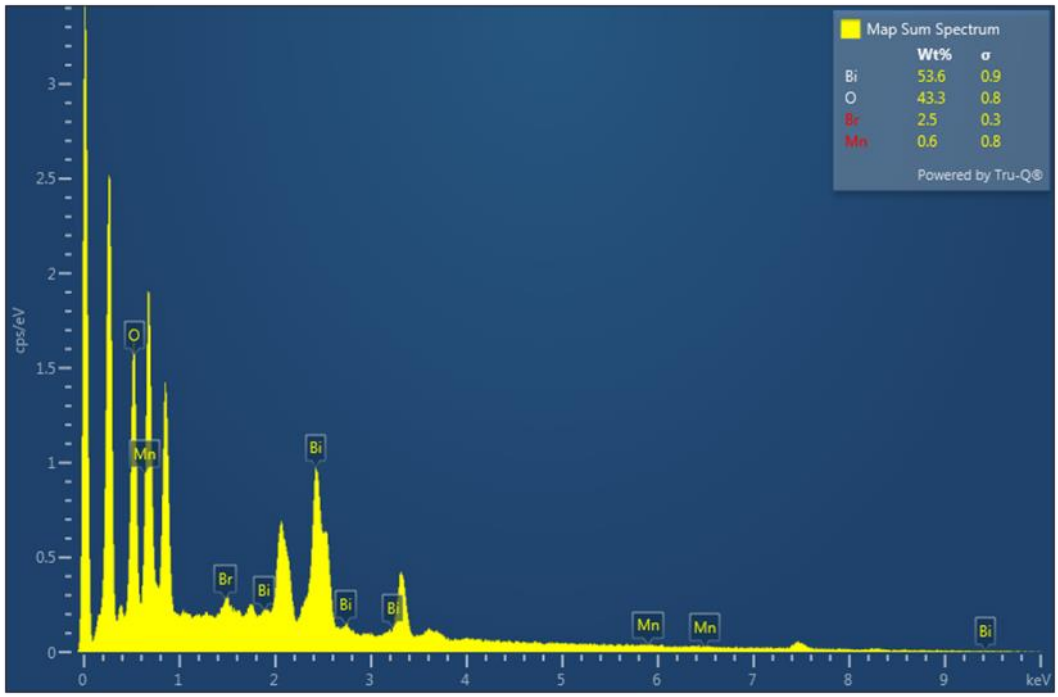

Figure S19: EDX spectra of the Mn-Bi_3O_4Br/NF electrode after post-OER CA at 1.6 V for over 12 h. .

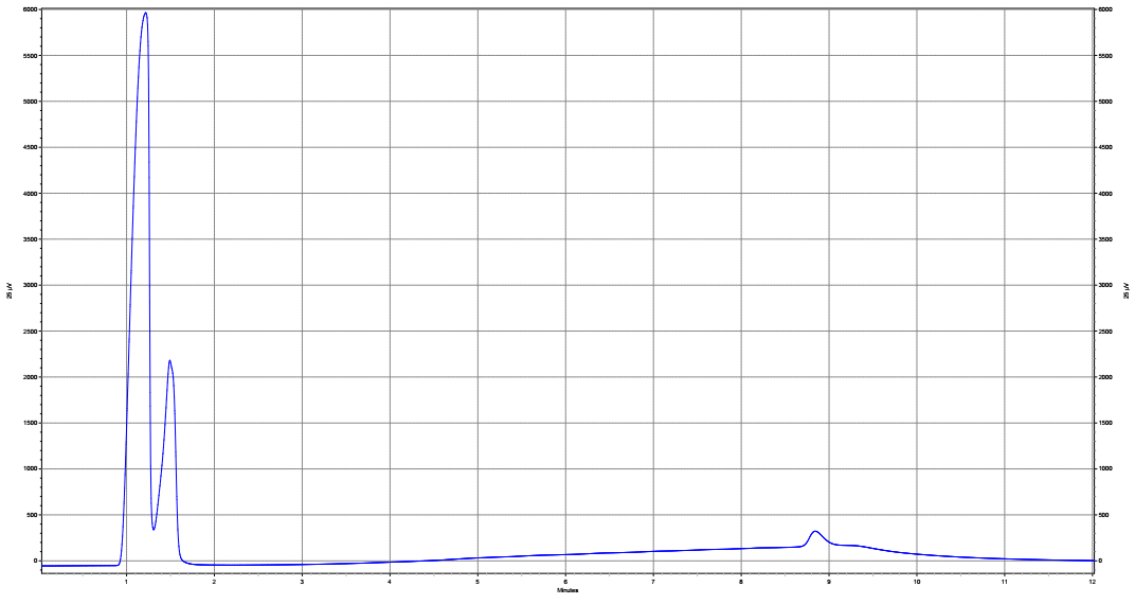

Figure S20: GC chromatogram of the evolved H_2 and O_2 from the full cell electrolyser developed with Mn-Bi_3O_4Br(+)/(-)GR after electrolysis at 2.5 V. The peak at retention time 1.1 and 1.3 is of H_2 and N_2, while the O_2 peak appeared at retention time 8.8.

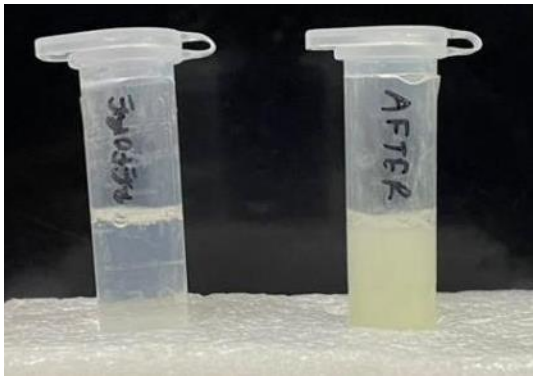

Figure S21: A wet analysis of the electrolyte after 12 h OER CA at 1.6 V CA with Mn-Bi_3O_4Br. Left: pre-OER CA electrolyte and right: pale yellow AgBr precipitate (right) obtained by addition of $AgNO_3$ solution (after acid treatment).

References

(1) Ye, Z.; Li, T.; Ma, G.; Dong, Y.; Zhou, X. Metal-Ion (Fe, V, Co, and Ni)-Doped MnO_2 Ultrathin Nanosheets Supported on Carbon Fiber Paper for the Oxygen Evolution Reaction. *Adv. Funct. Mater.* **2017**, *27* (44), 1704083.
(2) Zhuang, Q.; Ma, N.; Yin, Z.; Yang, X.; Yin, Z.; Gao, J.; Xu, Y.; Gao, Z.; Wang, H.; Kang, J.; Xiao, D.; Li, J.; Li, X.; Ma, D. Rich Surface Oxygen Vacancies of MnO2 for Enhancing Electrocatalytic Oxygen Reduction and Oxygen Evolution Reactions. *Adv. Energy Sustainability Res.* **2021**, *2* (8), 2100030.
(3) Luo, X.-F.; Wang, J.; Liang, Z.-S.; Chen, S.-Z.; Liu, Z.-L.; Xu, C.-W. Manganese oxide with different morphology as efficient electrocatalyst for oxygen evolution reaction. *Int. J. Hydrog. Energy* **2017**, *42* (10), 7151-7157.
(4) Yang, Y.; Su, X.; Zhang, L.; Kerns, P.; Achola, L.; Hayes, V.; Quardokus, R.; Suib, S. L.; He, J. Intercalating MnO2 Nanosheets With Transition Metal Cations to Enhance Oxygen Evolution. *ChemCatChem* **2019**, *11* (6), 1689-1700.
(5) Pujari, R. B.; Gund, G. S.; Patil, S. J.; Park, H. S.; Lee, D.-W. Anion-exchange phase control of manganese sulfide for oxygen evolution reaction. *J. Mater. Chem. A* **2020**, *8* (7), 3901-3909.
(6) Rauti, R.; Musto, M.; Bosi, S.; Prato, M.; Ballerini, L. Properties and behavior of carbon nanomaterials when interfacing neuronal cells: How far have we come? *Carbon* **2019**, *143*, 430-446.
(7) Singh, H.; Marley-Hines, M.; Chakravarty, S.; Nath, M. Multi-walled carbon nanotube supported manganese selenide as a highly active bifunctional OER and ORR electrocatalyst. *J. Mater. Chem. A* **2022**, *10* (12), 6772-6784.
(8) Antoni, H.; Xia, W.; Masa, J.; Schuhmann, W.; Muhler, M. Tuning the oxidation state of manganese oxide nanoparticles on oxygen- and nitrogen-functionalized carbon nanotubes for the electrocatalytic oxygen evolution reaction. *Phys. Chem. Chem. Phys.* **2017**, *19* (28), 18434-18442.
(9) Menezes, P. W.; Walter, C.; Hausmann, J. N.; Beltrán-Suito, R.; Schlesiger, C.; Praetz, S.; Yu. Verchenko, V.; Shevelkov, A. V.; Driess, M. Boosting Water Oxidation through In Situ Electroconversion of Manganese Gallide: An Intermetallic Precursor Approach. *Angew. Chem. Int. Ed.* **2019**, *58* (46), 16569-16574.
(10) Menezes, P. W.; Walter, C.; Chakraborty, B.; Hausmann, J. N.; Zaharieva, I.; Frick, A.; von Hauff, E.; Dau, H.; Driess, M. Combination of Highly Efficient Electrocatalytic Water Oxidation with Selective Oxygenation of Organic Substrates using Manganese Borophosphates. *Adv. Mater.* **2021**, *33* (9), 2004098.